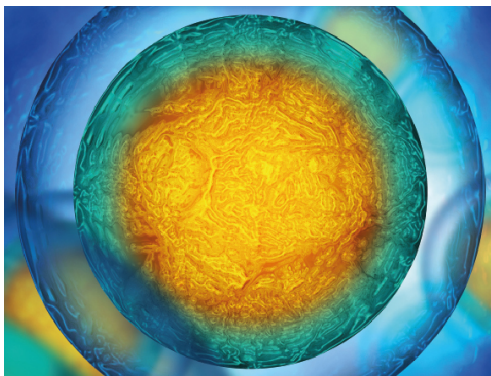


PAPER • OPEN ACCESS

## A minimal robophysical model of quadriflagellate self-propulsion

To cite this article: Kelimar Diaz *et al* 2021 *Bioinspir. Biomim.* **16** 066001

View the [article online](#) for updates and enhancements.



Your publishing choice in all areas of biophysics research.

Start exploring the collection—download the first chapter of every title for free.

# Bioinspiration & Biomimetics

**OPEN ACCESS****PAPER**

## A minimal robophysical model of quadriflagellate self-propulsion

**RECEIVED**  
14 March 2021**REVISED**  
14 July 2021**ACCEPTED FOR PUBLICATION**  
6 August 2021**PUBLISHED**  
1 September 2021

Original content from this work may be used under the terms of the [Creative Commons Attribution 4.0 licence](#).

Any further distribution of this work must maintain attribution to the author(s) and the title of the work, journal citation and DOI.



Kelimar Diaz<sup>1,2</sup>, Tommie L Robinson<sup>2</sup>, Yasemin Ozkan Aydin<sup>2,3</sup>, Enes Aydin<sup>2</sup>, Daniel I Goldman<sup>2</sup> and Kirsty Y Wan<sup>4,\*</sup>

<sup>1</sup> Interdisciplinary Graduate Program in Quantitative Biosciences, Georgia Institute of Technology, Atlanta, GA 30332, United States of America

<sup>2</sup> School of Physics, Georgia Institute of Technology, Atlanta, GA 30332, United States of America

<sup>3</sup> Department of Electrical Engineering, University of Notre Dame, Notre Dame, IN 46556, United States of America

<sup>4</sup> Living Systems Institute & College of Engineering, Mathematics, and Physical Sciences, University of Exeter, EX4 4QD, United Kingdom

\* Author to whom any correspondence should be addressed.

**E-mail:** [daniel.goldman@physics.gatech.edu](mailto:daniel.goldman@physics.gatech.edu) and [k.y.wan2@exeter.ac.uk](mailto:k.y.wan2@exeter.ac.uk)

**Keywords:** swimming, gait, robot, algae, bio-inspired, cilia, legged locomotion

Supplementary material for this article is available [online](#)

### Abstract

Locomotion at the microscale is remarkably sophisticated. Microorganisms have evolved diverse strategies to move within highly viscous environments, using deformable, propulsion-generating appendages such as cilia and flagella to drive helical or undulatory motion. In single-celled algae, these appendages can be arranged in different ways around an approximately 10  $\mu\text{m}$  long cell body, and coordinated in distinct temporal patterns. Inspired by the observation that some quadriflagellates (bearing four flagella) have an outwardly similar morphology and flagellar beat pattern, yet swim at different speeds, this study seeks to determine whether variations in swimming performance could arise solely from differences in swimming gait. Robotics approaches are particularly suited to such investigations, where the phase relationships between appendages can be readily manipulated. Here, we developed autonomous, algae-inspired robophysical models that can self-propel in a viscous fluid. These macroscopic robots (length and width = 8.5 cm, height = 2 cm) have four independently actuated ‘flagella’ (length = 13 cm) that oscillate under low-Reynolds number conditions ( $\text{Re} \sim \mathcal{O}(10^{-1})$ ). We tested the swimming performance of these robot models with appendages arranged two distinct configurations, and coordinated in three distinct gaits. The gaits, namely the pronk, the trot, and the gallop, correspond to gaits adopted by distinct microalgal species. When the appendages are inserted perpendicularly around a central ‘body’, the robot achieved a net performance of 0.15–0.63 body lengths per cycle, with the trot gait being the fastest. Robotic swimming performance was found to be comparable to that of the algal microswimmers across all gaits. By creating a minimal robot that can successfully reproduce cilia-inspired drag-based swimming, our work paves the way for the design of next-generation devices that have the capacity to autonomously navigate aqueous environments.

## 1. Introduction

The capacity for self-generated movement is a distinguishing feature of most living organisms. In the macroscopic world, locomotion is typically associated with inertia [1], though recent work has revealed the dominance of friction in terrestrial movement

[2, 3]. On the other hand, movement at the microscopic scale is subject to low Reynolds number physics, and cannot take advantage of inertial coasting. Without motility, a bacterium can only coast a minuscule distance an order of magnitude below the Ångström scale [4]. Over billions of years of evolution, microorganisms have become adept at

swimming, evolving distinct mechanisms for powering and maintaining self-propulsion through a fluid, often achieving speeds of several tens of cell-body lengths per second. This active motility confers a significant survival advantage, allowing microbes to navigate freely toward regions or locations where nutrients or resources are more plentiful [5]. Depending on the arrangement and number of locomotor appendages, single cells can execute swimming gaits that are surprisingly reminiscent of animals. For example, the model biflagellate alga *Chlamydomonas* actuates two equal-length flagella in a breaststroke [6], while quadriflagellate algae (single cells with four flagella) exhibit distinctive quadrupedal gaits such as the trot or the gallop [7] (figures 1(A) and (B)).

In recent years, advances have been made in understanding the biomechanics of microswimming. Here, the Reynolds number is small,  $Re = UL/\nu$ , where  $L$  is a typical lengthscale of the swimmer,  $U$  a typical velocity scale, and  $\nu$  is the kinematic viscosity of the fluid. Equally important is the oscillatory Reynolds number  $Re^{osc} = L^2\omega/\nu$  [8], where  $\omega$  is the typical stroke frequency (which sets a tip velocity of  $\omega L$ ). When both are small, flows are then governed by the Stokes equations:  $0 = \nabla p - \mu \nabla^2 \mathbf{v}$  and  $\nabla \cdot \mathbf{v} = 0$  (where  $\mathbf{v}$  and  $p$  are the flow and pressure fields), and have no explicit time-dependence. Microorganisms are able to break time-reversal symmetry using non-reciprocal strokes or body deformations, often involving whip-like appendages called cilia and flagella [4, 9]. While bacteria make use of rigid helical flagella [10], eukaryotes actuate motile cilia which produce asymmetric waves of propulsion [11, 12]. For a microorganism oscillating a 10  $\mu\text{m}$  flagellum at 50 Hz,  $Re \sim 10^{-3}$ , and  $Re^{osc} \sim 10^{-2}$ . One further asymmetry is required for forward propulsion [13]: in living cells this can be achieved by shape asymmetry, which is ensured by the slender aspect ratio of all cilia and flagella (about 100). Rigid colloidal particles can also self-propel by diffusiophoresis without shape changes by generating concentration gradients [14]. A rod sweeping through a fluid in the direction perpendicular to the axis of the rod experiences approximately twice the drag compared to when it is moved in the parallel direction [15]. Organisms across all scales have been found to exploit this basic anisotropy for locomotion [3, 16, 17].

Despite the adoption of cilia and flagella as a common propulsion mechanism, the microscale locomotion strategies of microorganisms have diversified significantly across different phyla [18]. It is not well-understood why different gaits exist nor how they are coordinated. For centuries, locomotor gaits have been studied in the context of terrestrial animals, where the sequences of relative movement sustained by subsets of limbs or legs have fascinated researchers. In vertebrates, gaits are thought to be generated by central pattern generators [19]. But how

can orderly, deterministic appendage coordination occur in single cells in the absence of nervous control [18, 20]? Recent theoretical and experimental work have shown that dynamic gait selection, at least in flagellates, appears to be an active and species-dependent process driven by intracellular and mechanical coupling [20, 21]. Notably, distinct quadriflagellates can self-propel at different speeds despite an apparently identical arrangement of flagella around the cell body [7, 22]. Since the ancestral form of the green algal lineage may have been a unicell with four flagella [23], there is much incentive to understand the precise mechanisms of appendage coordination in such systems.

In the quest to address these open questions of movement control, extant organisms can provide only a limited parameter space of possibilities in terms of size, shape, beat frequency, etc, often making it challenging to investigate certain configurations or physical regimes. Theoretical and computational approaches have been instrumental in shaping our understanding of active propulsion [15, 24], but these can be computationally expensive or reliant on simplifying assumptions. Meanwhile robophysical modelling has emerged as a powerful and versatile technique for elucidating organismal behavior by engineering customised configurations that can be easily tested in controlled laboratory settings [25–27]. The revolution in robophysical modelling has been driven in part by low cost electronics (motors, microcontrollers), and increasingly accessible control technologies that can complement theoretical modelling to provide real biological insights [26, 28]. However, trying to model cell movement is a significant conceptual challenge when working *at the microscale*. Even though increasingly controllable micro- and nano-devices have been fabricated to mimic the locomotive behaviors of biological swimmers [29, 30], these are overwhelmingly driven by external magnetic, electric or chemical fields. Magnetic fields are often unable to deliver the fine spatial control, required to independently actuate individual artificial cilia in a given array or network though there have been some recent progress in device miniaturisation [31]. As theoretical representations of flagellates, artificial swimmers and microrobots, minimal models based on a small number of moving components (beads, rods) have yielded significant insights into the effect of gait coordination on self-propulsion and motility [32–35]. Meanwhile, more realistic models of propulsive organelles that account for filament elasticity and shape have also been developed for single or arrays of cilia [36–38], but these approaches have not yet been applied to evaluate the influence of swimming *gait* in freely-moving multiflagellates.

The intrinsic limits of device manufacture at small scales severely undermines the suitability of microbots as realistic models of cell motility. To understand the influence of gait on self-propulsion

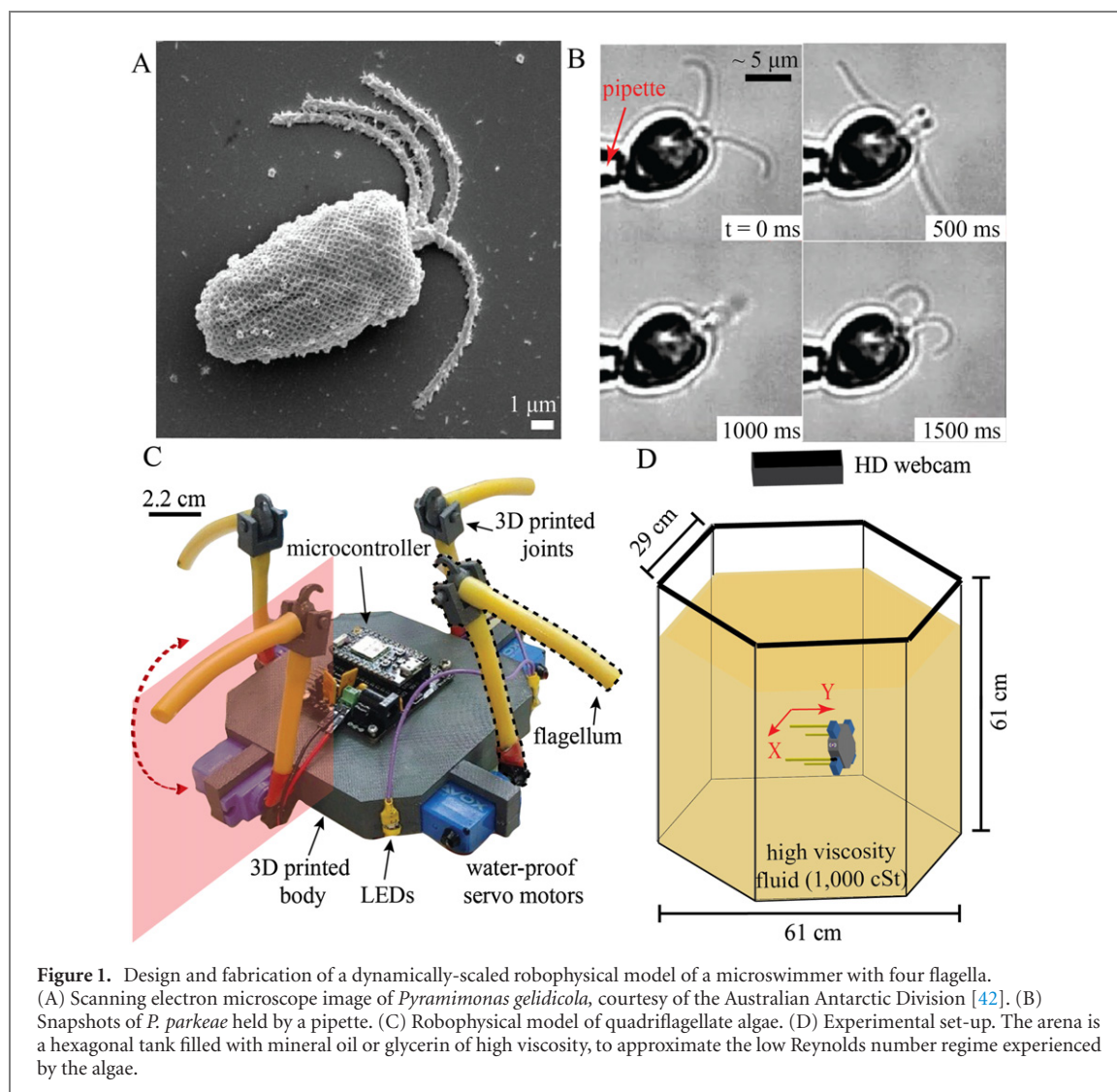


**Figure 1.** Design and fabrication of a dynamically-scaled robophysical model of a microswimmer with four flagella. (A) Scanning electron microscope image of *Pyramimonas gelidicola*, courtesy of the Australian Antarctic Division [42]. (B) Snapshots of *P. parkeae* held by a pipette. (C) Robophysical model of quadriflagellate algae. (D) Experimental set-up. The arena is a hexagonal tank filled with mineral oil or glycerin of high viscosity, to approximate the low Reynolds number regime experienced by the algae.

at low-Reynolds number, our goal is to build a dynamically-scaled robophysical model which is truly *self-powered*, where the movement of individual locomotor appendages can be prescribed and controlled independently. In contrast to traditional ‘microrobots’, the larger size allows us to explore and take advantage of increasingly sophisticated electronics and control architectures [39, 40]. We can readily reprogram these ‘roboflagellates’ to execute specific swimming gaits, making them well suited to testing theories of bio-inspired and autonomous locomotion at low-Reynolds number. This paper is organised as follows: We first identified and measured the relative swimming performance of three species of quadriflagellate algae that exhibit near-identical morphology but distinct swimming speeds. Next we built an O(10)cm robot that can self-propel in high-viscosity fluid when mimicking the asymmetric beat pattern of the algal flagella, verifying that low-Reynolds number kinematics are recapitulated. By arranging the robotic flagella in one of two possible configurations (parallel or perpendicular) relative to a central ‘cell body’, we imposed and tested three distinct flagellar actuation patterns

(gaits) that occur naturally in the algal flagellates, namely the pronk, the trot, and the gallop. In each case, we compared the hydrodynamic swimming performance of the robot to that of the corresponding algal species. Finally, we discuss the relevance of these results for understanding how functional differences in swimming performance may arise from morphologically similar structures, and highlight the implications of this from an eco-evolutionary perspective.

## 2. Methods

### 2.1. Microalgal culturing and imaging

Three species of algae (*Pyramimonas parkeae*, *Pyramimonas tetrahynchus* and *Carteria crucifera*) were cultured axenically according to previously published protocols [7, 20]. Free-swimming individuals were tracked in open microfluidic chambers using a high-speed camera (Phantom Vision Research). Brightfield imaging was conducted with 40× or 60× objectives using standard inverted microscopes (Leica DMI8 and Nikon T2000-U) under white light illumination. Free-swimming trajectories were obtained from high-speed videos in which single

cells crossed the focal plane, with the use of the open source software TrackMate (Fiji) [41]. Ten cells per species were used to determine the performance of each swimming gait (supplementary video 1 (<https://stacks.iop.org/BB/16/066001/mmedia>)).

Tracks in which cells performed transient gaits, tumbles, or changed directions were not used in this analysis. The body length of each cell was measured along the long axis (anterior-posterior) of the organism. An average body length of  $13.95 \pm 2.05 \mu\text{m}$ ,  $12.54 \pm 0.65 \mu\text{m}$ , and  $12.82 \pm 0.72 \mu\text{m}$  was found for *P. parkeae*, *P. tetrarhynchus* and *C. carteria* respectively.

## 2.2. A self-powered roboflagellate

We designed a dynamically-scaled robot to ensure that the robophysical model is self-powered and did not require external fields—all controllers and servos are fully self-contained (figure 1(C)). We performed robotic experiments in a highly viscous fluid (mineral oil, McMaster, 1000 cSt, product No. 1401K75) to approximate the low Reynolds number regime experienced by the algae (figure 1(D)). A subset of trials were conducted in glycerin (vegetable glycerin, Blue Water Chem Group, product No. B07FQWDTH7) of comparable viscosity to the mineral oil, to enable better visualisation and tracking of appendage movement. Each robot consisted of a 3D printed body (length and width = 8.5 cm, height = 2 cm) attached to four flagella that were independently actuated by waterproof servo motors (Savox, product No. SW0250MG, max torque of 3.5 kg/0.34 Nm, operating at 4.8 V). Each appendage was oriented such that the stroke lies in the plane perpendicular to the body (figure 1(C)). Foam (FOAMULAR Insulating Sheathing (IS) XPS Insulation) was attached on the robot body to achieve neutral buoyancy, allowing it to swim untethered. Commanded appendage positions were achieved using a micro-controller (Photon, Particle, part ID: PHOTONH) that allowed actuation of the robot with the use of Wi-Fi. The microcontroller and each motor were connected via an IOT Servo Shield (Actuonix, part ID: IOT-SHIELD-PHOTON), a circuit board specific to our micro controller. Four LEDs were placed on the 3D printed body to facilitate tracking. The robot was powered with three lithium ion polymer batteries (3.7 V, 2500 mAh), each powering directly the micro controller, the motors, and any attached LEDs. With this micro controller, the robots were able to sustain self-propulsion over approximately one hour.

## 2.3. Actuation of robotic flagella

Inspired by the flagellar beating waveform of the organisms, we implemented a simple two-link robotic flagellum connected via a 3D printed joint (figure 2). Each robotic appendage (length = 6.5 cm, diameter

= 3.1 mm, polypropylene-based thermoplastic elastomer) could bend passively to break time-reversal symmetry, without the need to actively prescribe the shape of the flagella over a beat cycle (figure 2(B)). No external control such as magnetic fields were used; our robot was completely open loop. Each gait maintained a constant phase difference between adjacent flagella set by prescribed joint angles of the proximal segment (figure 3, supplementary video 2). Each gait was uploaded to the microcontroller via Wi-Fi, allowing the controllers to actuate the motors. Unless otherwise specified, all gaits were prescribed with a flagellar beat frequency of 0.14 Hz.

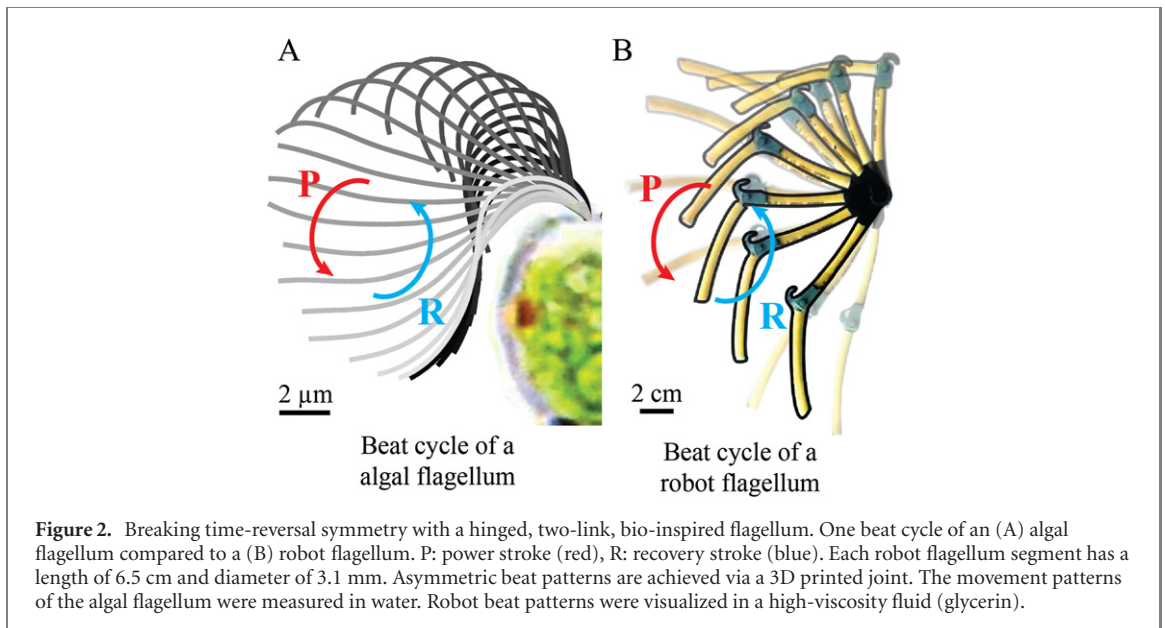
For the movement of the robot in mineral oil (kinematic viscosity  $\mu/\rho = 10 \text{ cm}^2 \text{ s}^{-1}$ ), the Reynolds number for the body (Re) was 0.14 ( $L = 3.8 \text{ cm}$ ,  $U = 0.38 \text{ cm s}^{-1}$ ), while the oscillatory Reynolds number  $\text{Re}^{\text{osc}}$  was 0.20 ( $L = 3.8 \text{ cm}$ ,  $\omega = 0.14 \text{ Hz}$ ). For the experiments conducted in glycerin (kinematic viscosity  $\mu/\rho = 11.83 \text{ cm}^2 \text{ s}^{-1}$ ),  $\text{Re} = 0.27$  ( $L = 6.89 \text{ cm}$ ,  $U = 0.40 \text{ cm s}^{-1}$ ), and  $\text{Re}^{\text{osc}} = 0.55$  ( $L = 6.89 \text{ cm}$ ,  $\omega = 0.14 \text{ Hz}$ ).

## 2.4. Prescribing the swimming gait in the roboflagellate

We imposed three distinct gaits on the robot similar to those observed in quadriflagellate algae—the pronk, the trot, and the gallop. The different coordination patterns were achieved by prescribing the phase differences between adjacent appendages. The resulting gait sequences were confirmed for an immobilised robot body, where the distance from each flagellum tip to the cell body was used as proxy for phase. In the pronk gait, all four appendages move simultaneously, without any phase difference ( $\varphi = 0^\circ$ ) between adjacent flagella (figure 3(A)). The trot gait is defined by alternating pairs of flagella each of which is generating a pattern analogous to a breaststroke, with a phase difference of half a gait cycle ( $\varphi = 180^\circ$ ) (figure 3(B)). In the gallop gait, each appendage moves with a phase difference of a quarter-gait cycle relative to its neighbor (figure 3(C)). The directionality (clockwise (CW) or counter-clockwise (CCW)) of the gallop gait is determined by the phase difference ( $\varphi$ ) between the first appendage ( $m_1$ ) and an adjacent appendage ( $m_2$  or  $m_4$ ). We tested the gallop gait in both a CW ( $\varphi = 90^\circ$  between  $m_1$  and  $m_2$ ) and CCW ( $\varphi = 180^\circ$  between  $m_1$  and  $m_2$ ) direction. We imposed either a CW and CCW direction to investigate how chirality can affect the performance of the gallop gait.

## 2.5. Motion tracking

Due to the opacity of the oil, we attached lightweight LEDs to the robot's body to enable motion tracking. All LEDs were digitized using custom MATLAB algorithms. We approximated the center of geometry of the robot by averaging the position of the LEDs over time. Then, we used the tracks to determine the distance traversed by the robot in units of body lengths



per beat cycle. A total of 9 trials were taken per gait, for each robot configuration. A trial was terminated either when the robot contacted a boundary, or if the LEDs were no longer visible as the robot slowly drifted downwards over time; this is due to the 3D material trapping fluid and increasing in mass. Each trial comprised 6–10 beat cycles per gait. In subsequent experiments, we used glycerin as an alternative high viscosity fluid to visualize and track movement of the flagella during active swimming. However, because glycerin is not a dielectric fluid, Wi-Fi connectivity was interrupted and the circuits were negatively affected. To resolve this, we substituted our microcontroller (Pro Trinket, Adafruit, product ID: 2000) and sealed the circuits with a gasket and a 3D printed cap. In glycerin, flagella kinematics were digitized using DLTdv8 [43].

### 3. Results and discussion

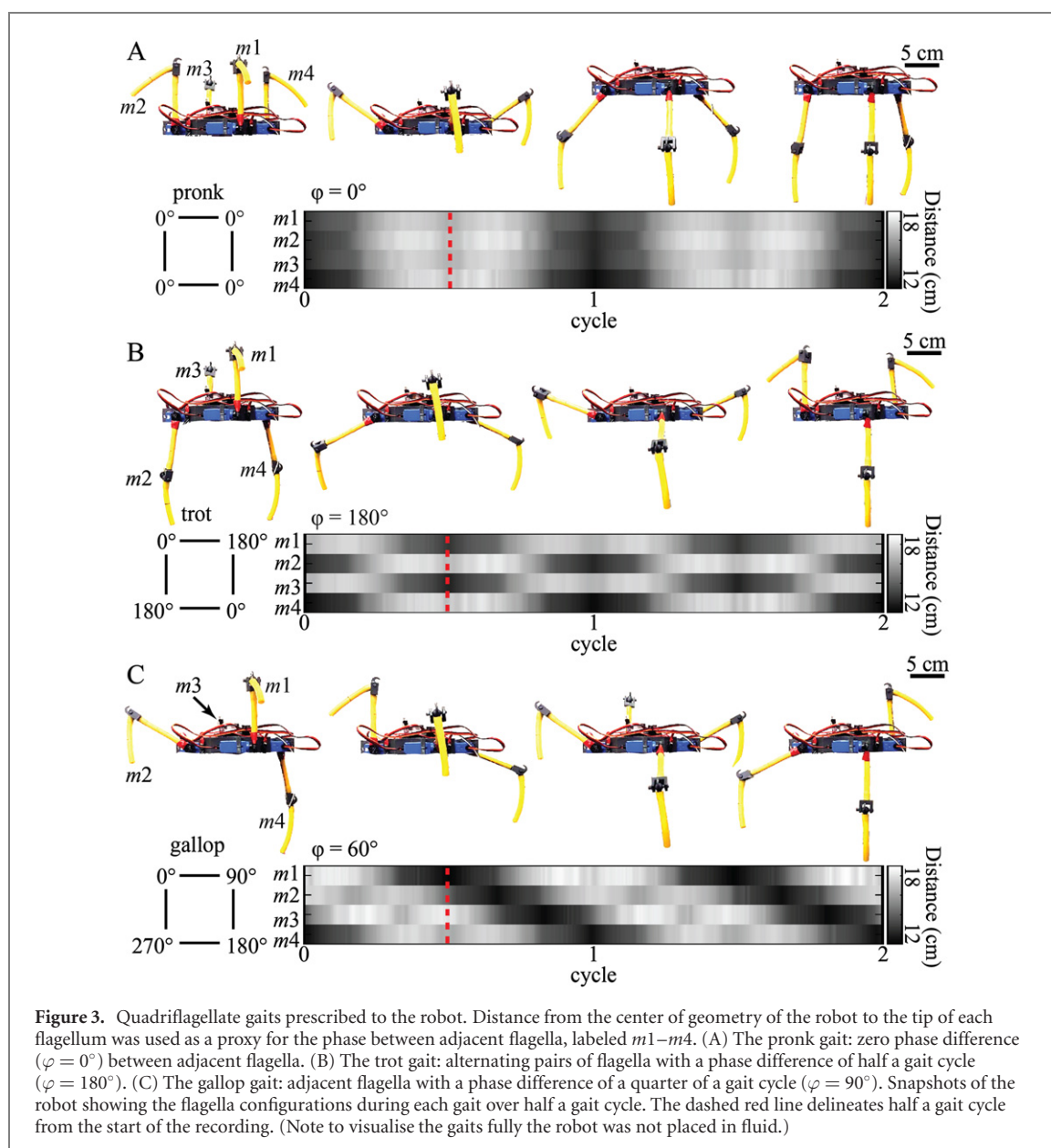
#### 3.1. The trot is the fastest gait in the algae

We identified the quadriflagellates as an ideal study group owing to their morphological diversity (in size, shape, aspect-ratio), and abundance in marine, terrestrial as well as freshwater habitats. A key trait among quadriflagellate genera is the arrangement or insertion of flagella around the anterior of the cell [23, 44]. Here we take advantage of this diversity to compare the swimming behavior of three species (*P. tetrahynchus*, *P. parkeae*, and *C. crucifera*) that employ three distinct gaits—respectively the pronk, the trot, and the gallop (supplementary video 1). We conjecture that inter-species differences in quadriflagellate swimming performance can be attributed to differences in gait alone—where the same basic stroke is applied to ensembles of appendages but according to distinct phase relationships.

Two of these algae belong to the genus *Pyramimonas*, a Prasinophyte algae belonging to an early diverging class which is thought to have given rise to the core chlorophyte algae, comprising species with two, four, eight, or up to sixteen flagella [7, 45]. Four flagella of identical length and beat pattern emerge from a deep anterior groove or pit in the cell body. The third species, *C. crucifera*, is a Volvocalean flagellate that is closely related to the model biflagellate *Chlamydomonas*. Despite this phylogenetic divergence, all three species are similar in body size and flagellar morphology, and appear obovoid (egg-shaped) to cordate (heart-shaped) in side profile [46, 47].

In all three cases, cells swim smoothly flagella-first (puller-type) at speeds of  $\mathcal{O}(100) \mu\text{m s}^{-1}$ . The translational motion is coupled to an axial rotation to produce swimming along helical trajectories [48]. Abrupt gait transitions can occur either spontaneously or when triggered by mechanical contact, during which the flagella are directed to the front of the cell in a so-called shock-response [49]. Cells can also reversibly stop and start swimming, when all or some of the flagella transiently cease to beat [20].

In all cases, free-swimming trajectories are super-helical, where small-scale swirls at the cell-scale are produced by the periodic flagellar oscillations. Three representative tracks, projected onto the focal plane, are shown in figures 4(A), (C) and (E). Using these tracks, we estimated for each of the three gaits the displacement per cycle, including the cumulative displacement as a function of phase during the beat cycle (figure 4(G)) as well as the mean forward progress per complete cycle (figure 4(H)). Measured swimming speeds were  $126 \pm 24 \mu\text{m s}^{-1}$  for the pronk,  $408 \pm 46 \mu\text{m s}^{-1}$  for the trot, and  $127 \pm 25 \mu\text{m s}^{-1}$  for the gallop. Our results show that



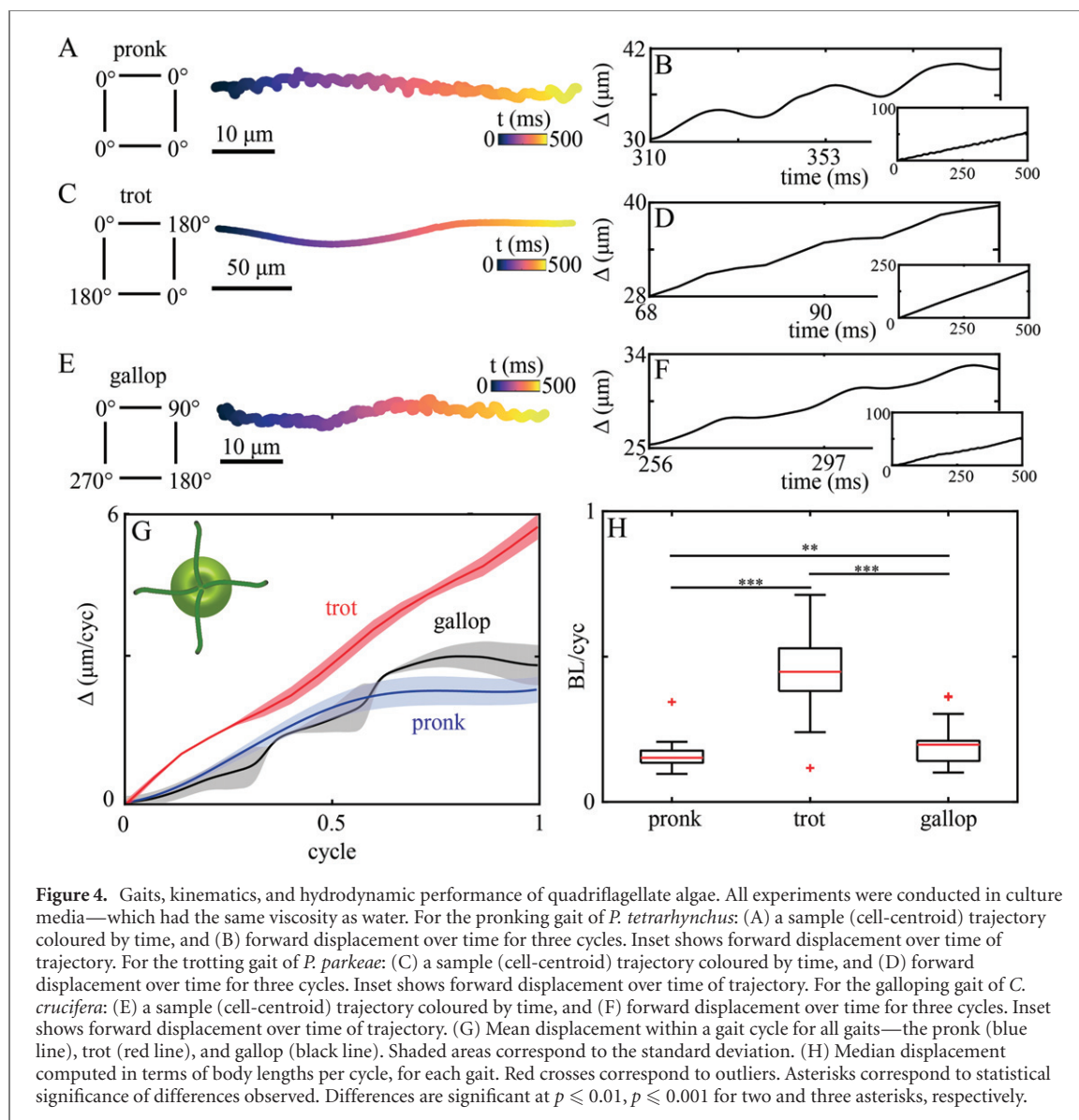
the trot gait is the fastest gait in the microalgae. Meanwhile the prong and gallop gaits lead to comparable propulsion speeds.

### 3.2. A hinged flagellum breaks time-reversal symmetry

We first confirmed that our robophysical model resides in a low-Reynolds number regime by attaching 3D-printed rigid (unhinged, length = 13 cm) flagella to the body, and actuating these with both a time-symmetric as well as a time-asymmetric stroke pattern. To create a time-asymmetric stroke, we increased the beating frequency of the recovery stroke. Due to the rotational position based control of the motors, changes in the frequency were achieved by changing the rate at which joint angles were prescribed. The recovery stroke frequency was varied from 0.07 Hz to 0.21 Hz (supplementary video 3). As expected,

reciprocal strokes produced negligible net swimming in both cases. For a time-symmetric pattern, the net displacement in the direction of movement after one complete cycle was  $0.38 \pm 0.40$  cm ( $0.05 \pm 0.05$  BL) using the prong gait (figure 5(A)). When the stroke frequency was increased, and consequently Reynolds number, the displacement of the robot increased (figure 5(B)). Thus, at higher beat frequencies the system can reach intermediate Reynolds numbers. Hereafter, we use a flagella beat frequency of 0.14 Hz to ensure inertial effects remain negligible.

With hinged instead of rigid flagella (figure 2(B)), the robot became capable of net forward propulsion. Each gait cycle can be characterized by a power stroke during which the robot gains distance, and a recovery stroke during which it loses distance. We first set out to test the effect of flagella ‘waveform’ on swimming performance, this is expected to scale approximately with stroke amplitude [50, 51].



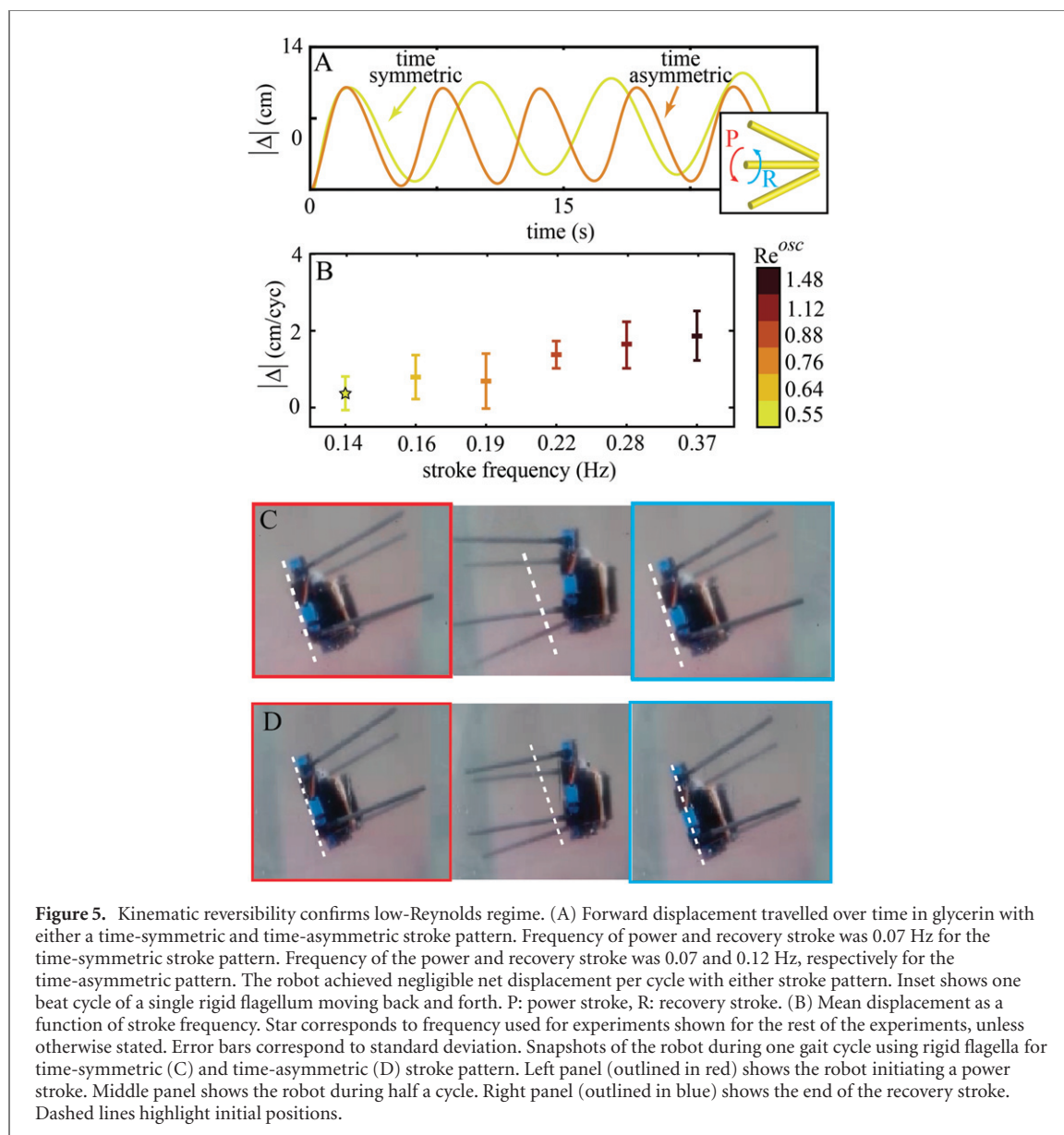
### 3.3. Flagellar undulation pattern affects swimming performance

We implemented two distinct flagellar undulation patterns—as defined by the maximal sweep range of the segments. For simplicity and to prevent axial rotation, we reduced our quadriflagellate robot to a biflagellate robot, by removing one pair of flagella (supplementary video 4). The remaining pair of flagella was programmed to follow a breaststroke pattern (figure 6(A)). We prescribed and compared the swimming performance for two different sets of motor angles for the proximal segment: (i)  $[0^\circ, 180^\circ]$ , and (ii)  $[45^\circ, 135^\circ]$  (figure 6(A) inset). The motion of the distal segment always follows passively, with the hinge breaking time-reversal symmetry. We tracked the flagella ‘waveform’ in the two cases and calculated the angles generated by each flagellum segment over time (from motor to joint and from joint to tip, figure 6(A)). The two sweep amplitudes produced two distinct gaits in the  $\theta_1$ – $\theta_2$  shape space figure 6(B).

A reduced sweep range results in a higher beat frequency ( $\omega = 0.14$  Hz for motor angles of  $[0^\circ, 180^\circ]$ , and  $\omega = 0.41$  Hz for motor angles of  $[45^\circ, 135^\circ]$ ). The rescaled displacement shows swimming performance increases with stroke amplitude (figure 6(C)). The larger-amplitude breaststroke achieves a greater displacement after each gait cycle. This suggests that non-inertial locomotion is dictated by geometric mechanics, as shown previously in the case of infinitesimal deformations [50]. Here, movement is kinematic, and net displacement is determined largely by the gait and its associated low-dimensional properties [52].

### 3.4. Roboflagellate swimming performance depends on gait and appendage placement

To test if swimming performance is dominated by gait or by other factors such as flagellar stiffness or waveform compliance, we prescribed the gaits exhibited by each algae species to our roboflagellates. We explored the effect of varying appendage phase coordination

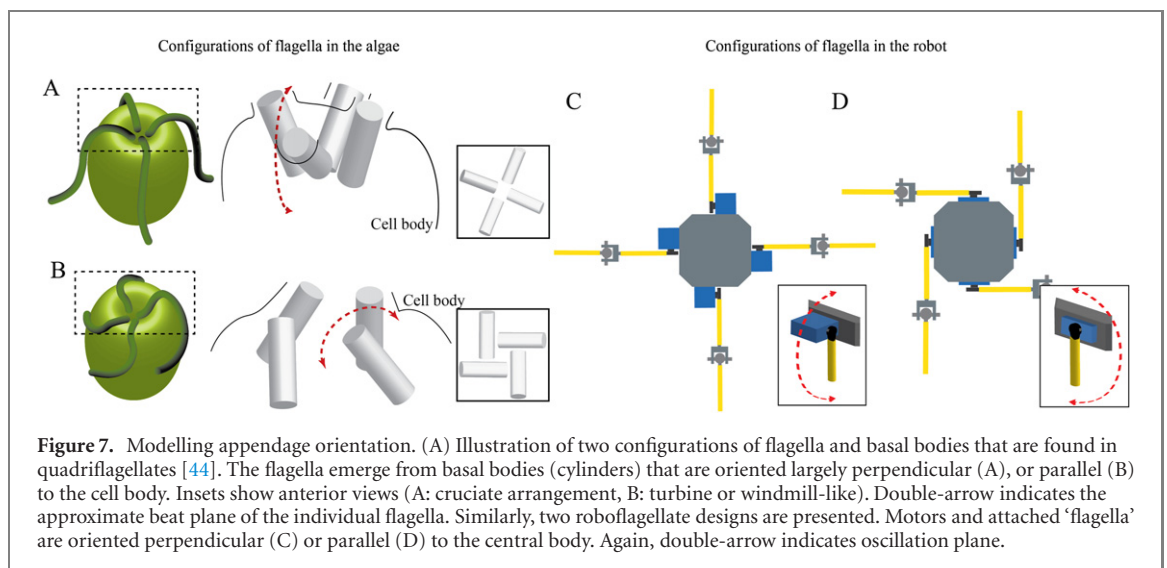
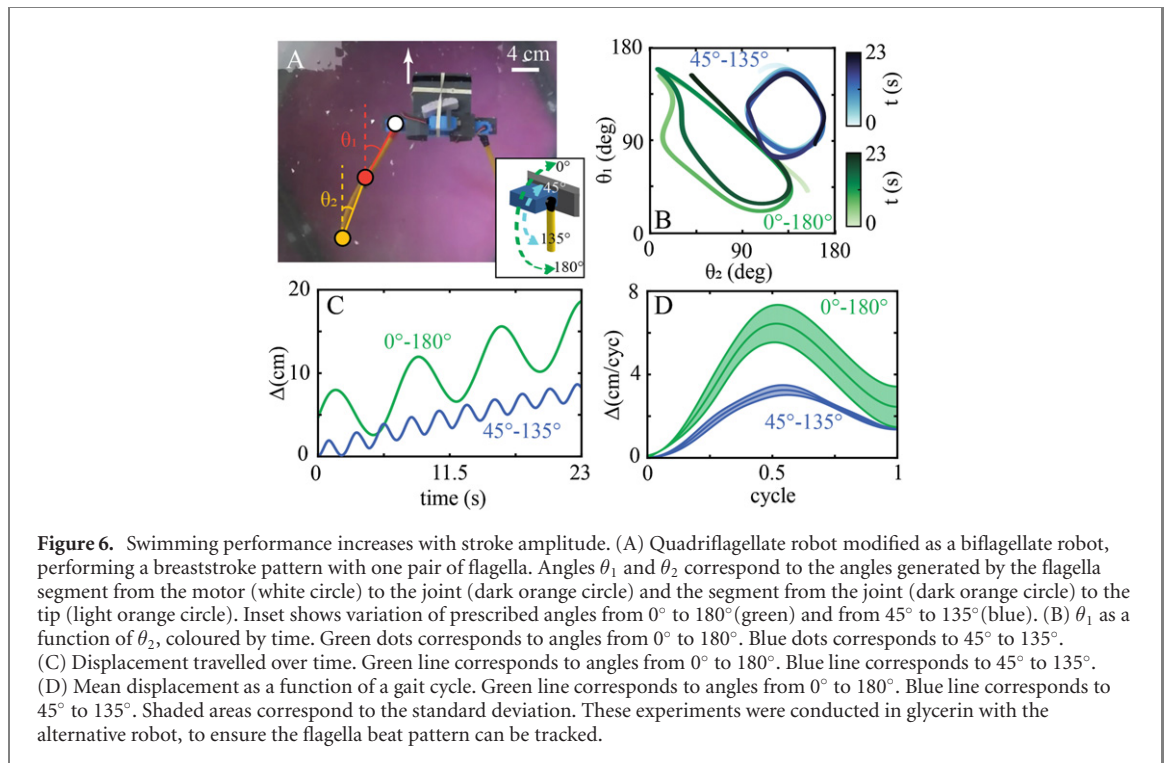


(gait) for two different configurations of four flagella, in which motors are positioned either in a parallel or a perpendicular orientation with respect to an identical body.

These configurations were modeled on naturally-occurring arrangements of basal bodies and flagella found in extant algal flagellates (figure 7). All three species of algae studied here correspond to configuration A, in which the approximate plane of flagellar beating is perpendicular to the surface of the robot body. The main difference is that when viewed from the anterior of the cell, the four flagella are inserted with a clockwise twist or offset for *Carteria*, but an anticlockwise offset for *Pyramimonas* [44]. Algal species reported to exhibit configuration B [44] were not available in culture and were not represented in the present study. Appendage coordination was prescribed in the robot by specifying the phase dif-

ferences between flagella, to produce each of the three gaits: pronk, trot, or gallop, as previously described (figure 3).

For the perpendicular configuration, example trajectories as well as the cumulative forward displacement over time for each gait are shown in figures 8(B), (C) and (E)–(J)). We also analyzed the detailed within-cycle dynamics for each gait (supplementary video 5). The pronk and both the CW gallop and CCW gaits produce significant forward displacement during the power stroke (up to 5.7 cm for the pronk, 4 cm and 2 cm for the CW and CCW gallops respectively after half a gait cycle), but also produce a significant backward displacement during the recovery stroke, generating overall small displacement from cycle to cycle ( $0.33 \pm 0.04$  BL/cyc,  $0.16 \pm 0.05$  BL/cyc, and  $0.15 \pm 0.08$  BL/cyc for the pronk, the CW gallop, and CCW gallop respectively). On the other hand, while the trot does not achieve a greater displacement (only 2.3 cm after half a gait cycle) than the pronk



or gallop during the power stroke, it loses a much smaller distance during the recovery stroke. This is because while one pair of flagella is moving toward the body and consequently producing backward motion, the other pair of flagella moves away from the body so as to resist this motion. This can also be observed in the trajectories, where the pronk and gallop gaits show backward motion, unlike the trot gait. Due to this, of the three gaits investigated the robot achieves the greatest hydrodynamic performance ( $0.6 \pm 0.08$  BL/cyc) using the trot gait (figure 8(K)), just as in the algae.

For the parallel configuration (supplementary video 6), example trajectories as well as the forward displacement over time for each gait can be seen in

figures 9(B), (C) and (E)–(J). Similar to the perpendicular configuration, the pronk gait allows the robot to gain a significant amount of distance during the power stroke (up to 5 cm after half a gait cycle) but also lose a significant amount of distance during the recovery stroke, generating little net displacement from cycle to cycle. The gallop gait in the CCW displays a similar oscillatory pattern, however there is a discrepancy between the CCW and CW gallops (5.3 cm after half a gait cycle for the CW gallop, but only 1 cm for the CCW gallop). This is likely due to rotation-translation coupling in the second configuration (in which the flagella are inserted in the CCW sense), generating significant motion laterally and causing axial rotation of the robot. Similar to the perpendicular robot, the trot gait advances less during

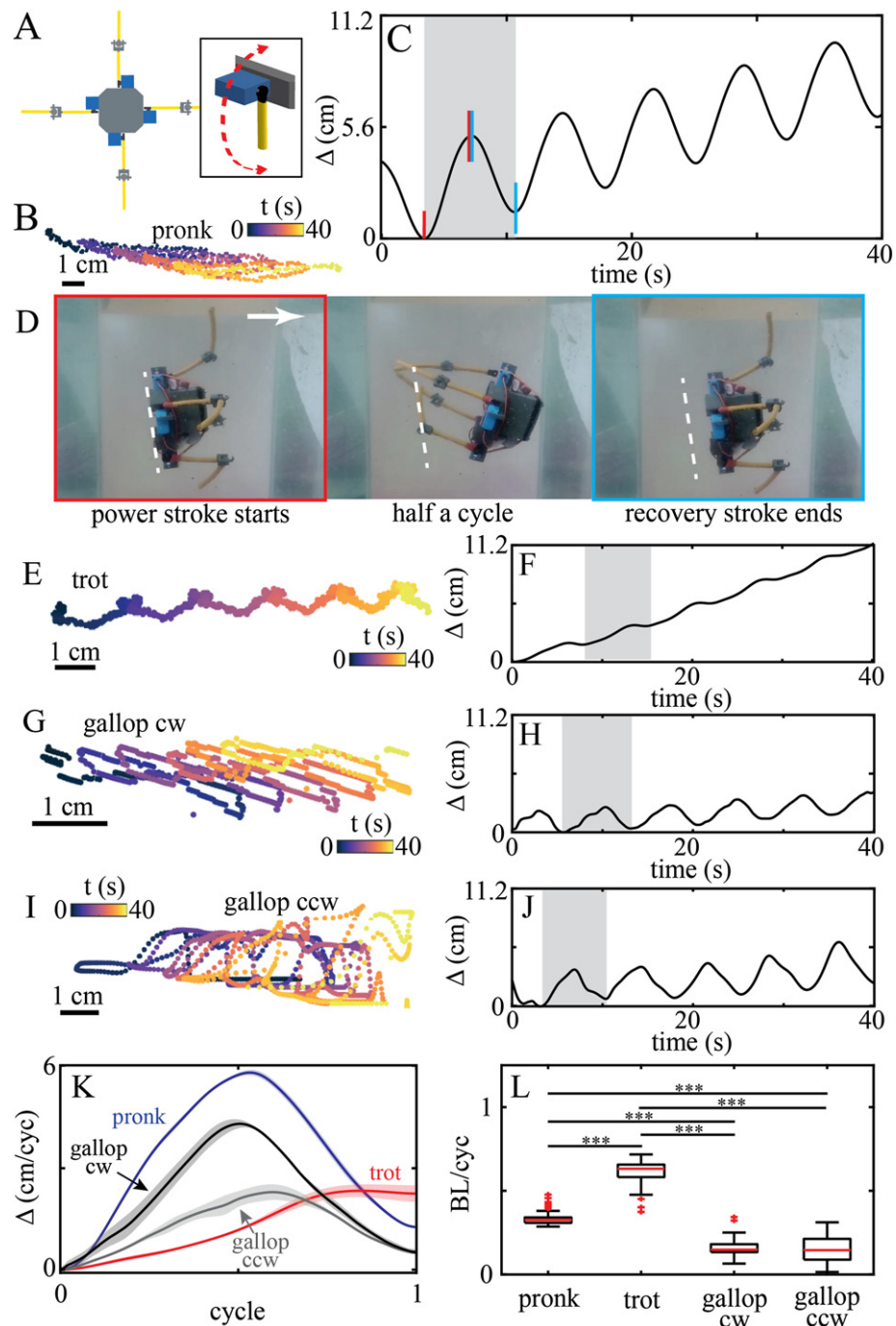


**Figure 8.** Swimming gait kinematics and performance for robot with flagella in the perpendicular orientation. (A) Diagram of robot with motors oriented perpendicular to the body. Inset illustrates beating plane. For the pronk gait, (B) shows a sample trajectory of the robot, coloured by time (5 cycles), and (C) the forward displacement travelled over time. For one gait cycle, red vertical lines highlight power stroke, and blue vertical lines highlight return stroke. (D) Snapshots of the robot during one cycle of the pronk gait. Left panel (outlined in red) shows the robot initiating a power stroke. Middle panel shows the robot during half a cycle. Right panel (outlined in blue) shows the robot completing the recovery stroke. (Arrow: swimming direction.) Trajectory of the robot during the trot gait, coloured by time (5 cycles) (E), and forward displacement travelled over time of the robot during the trot gait (F). Trajectory of the robot during the CW gallop gait, coloured by time (5 cycles) (G), and forward displacement travelled over time of the robot during the CW gallop gait (H). Trajectory of the robot during the CCW gallop gait, coloured by time (5 cycles) (I), and forward displacement travelled over time of the robot during the CCW gallop gait (J). (K) Mean displacement over a gait cycle for all gaits—the pronk (blue line), trot (red line), CW gallop (black line), and CCW gallop (gray line). Shaded areas correspond to the standard deviation. (L) Body length per cycle as a function of swimming gait. Red crosses correspond to outliers. Asterisks correspond to statistical significance of differences observed. Differences are significant at  $p \leq 0.001$  for three asterisks.

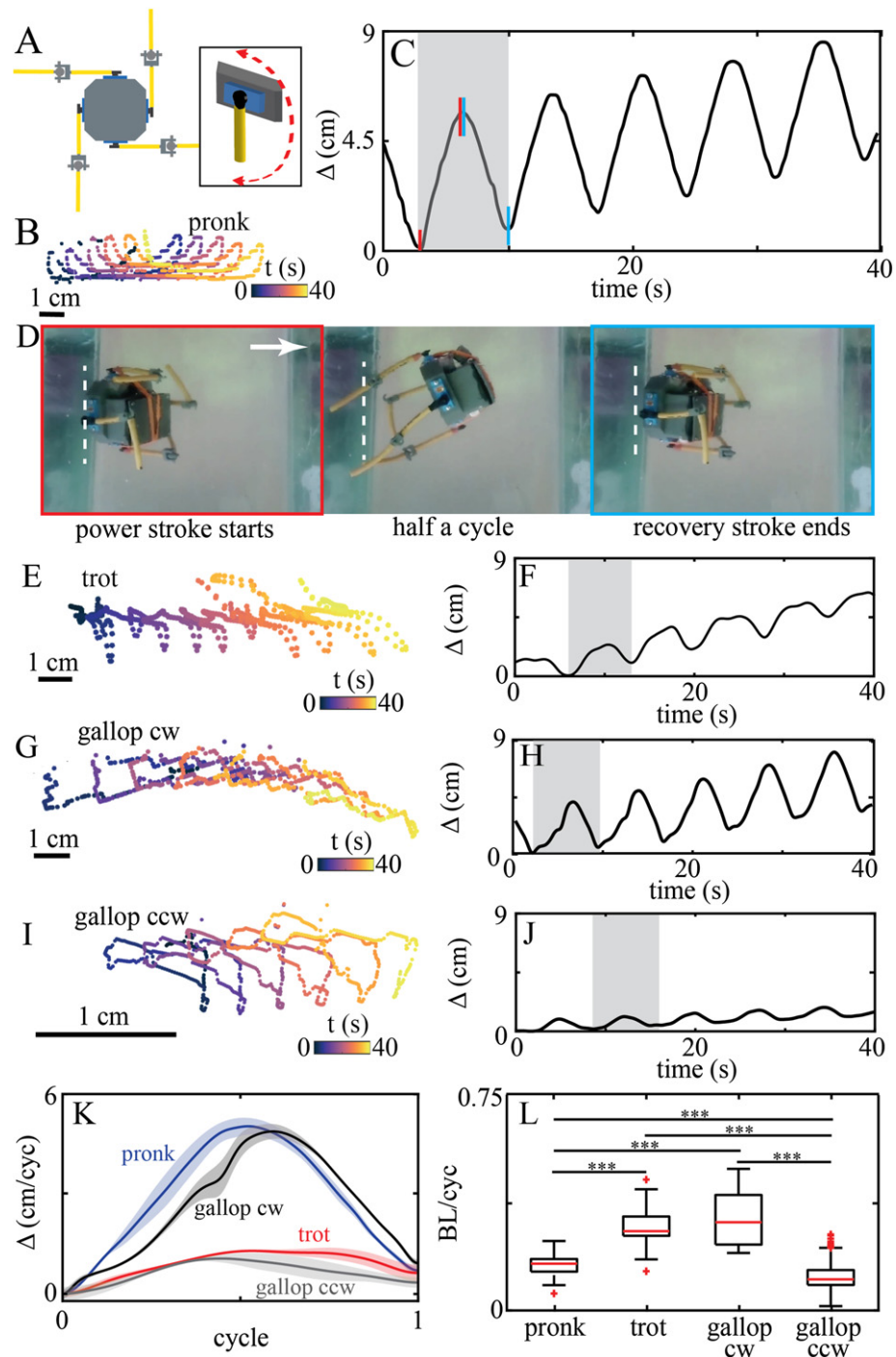
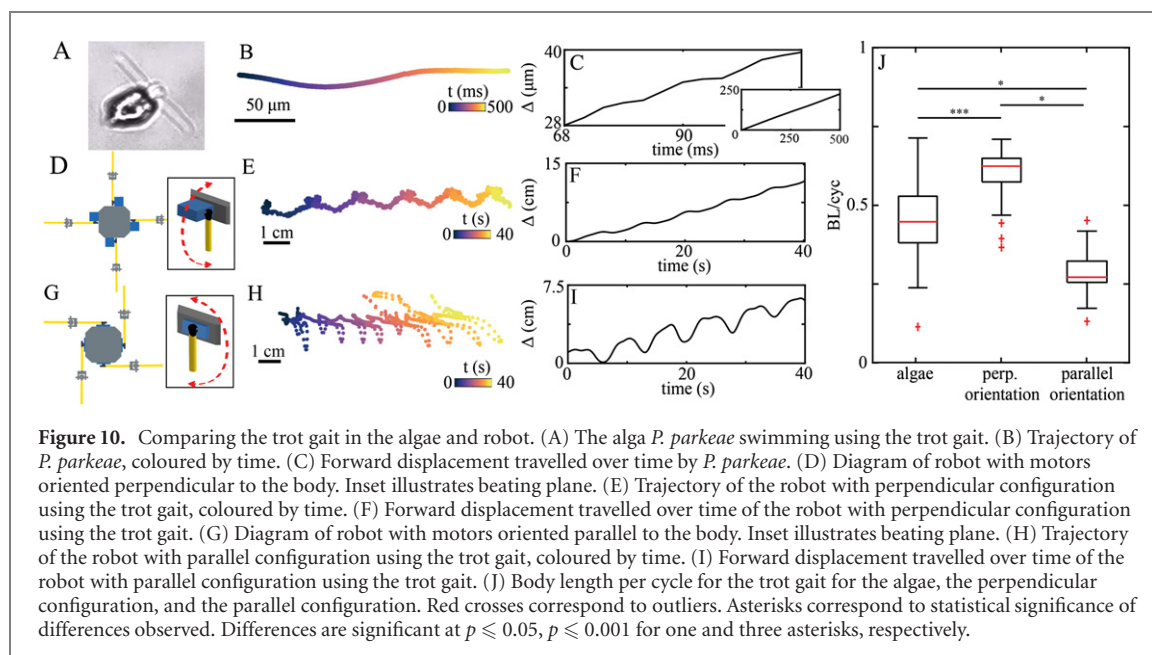


**Figure 9.** Swimming gait kinematics and performance for robot with flagella in the parallel orientation. (A) Diagram of robot with motors oriented perpendicular to the body. Inset illustrates beating plane. For the pronk gait, (B) shows a sample trajectory of the robot, coloured by time (5 cycles), and (C) the forward displacement travelled over time. For one gait cycle, red vertical lines highlight power stroke, and blue vertical lines highlight return stroke. (D) Snapshots of the robot during one cycle of the pronk gait. Left panel (outlined in red) shows the robot initiating a power stroke. Middle panel shows the robot during half a cycle. Right panel (outlined in blue) shows the robot completing the recovery stroke. (Arrow: swimming direction.) Trajectory of the robot during the trot gait, coloured by time (5 cycles) (E), and forward displacement travelled over time of the robot during the trot gait (F). Trajectory of the robot during the CW gallop gait, coloured by time (5 cycles) (G), and forward displacement travelled over time of the robot during the CW gallop gait (H). Trajectory of the robot during the CCW gallop gait, coloured by time (5 cycles) (I), and forward displacement travelled over time of the robot during the CCW gallop gait (J). (K) Mean displacement over a gait cycle for all gaits—the pronk (blue line), trot (red line), CW gallop (black line), and CCW gallop (gray line). Shaded areas correspond to the standard deviation. (L) Body length per cycle as a function of swimming gait. Red crosses correspond to outliers. Asterisks correspond to statistical significance of differences observed. Differences are significant at  $p \leq 0.001$  for three asterisks.



the power stroke (only 1.5 cm after half a gait cycle) and loses more distance during the recovery stroke, relative to the perpendicular configuration. The phasing between appendages in the trot gait again aids the robot in traversing a greater distance to cycle to cycle than the pronk ( $0.15 \pm 0.4$  BL/cyc), and also greater than the average of the CW and CCW gallop gaits ( $0.15 \pm 0.9$  BL/cyc). (We assume that by symmetry, this average between the two chiralities should cancel any rotational effects.) Thus, the trot remains a hydrodynamically effective gait for the parallel robot ( $0.26 \pm 0.08$  BL/cyc) (figure 9(K)).

We conclude that the swimming performance of the roboflagellate is highly sensitive to both gait and flagellar orientation (which defines the principal beat plane) of the flagella. It is possible that the organisms can access different regimes by controlling the 3D beat plane of their flagella, and that divergent flagellar placement evolved in different species as a result of different environmental selection pressures. In multicellular flagellates such as *Volvox*, nearby basal bodies (from which the flagella emerge) have rotated 90 degrees compared to the ancestral configuration found in the unicellular *Chlamydomonas*, likely to facilitate coordinated flagellar beating as an intact colony [7, 53].

### 3.5. Speed of roboflagellate is comparable to that of algae

The above results show that a change in flagellar configuration can significantly change the performance of a given swimming gait. Focusing only on the trot, we note that this gait yielded the highest hydrodynamic performance for the algae and for the perpendicular robot, (figure 10). Note that the speed of the algae trot gait is bounded above and below by that of the perpendicular and parallel robots.

In both robot configurations, significant axial rotation and lateral movement were observed in the

free-swimming trajectories (figures 10(E) and (H)) showing that our roboflagellates do not swim as smoothly as their algal counterparts (figure 10(B)). This is likely due to the discrepancy between the deformable stroke cycle of the continuous algal flagellum, compared to the angular movements of the two-link robot flagella. Additionally elastic elements in the algal cytoskeleton could play a role in gait stabilization by actively anchoring the flagella to the body [21, 54]. The cumulative displacement over time for a trotting cell and our perpendicular robot are comparable (figures 10(C) and (F)). Meanwhile the parallel configuration displays larger amplitude oscillations in which a greater distance gained during each the power stroke is negated during the subsequent recovery stroke (figure 10(I)). This is likely due to three-dimensional effects as mentioned above. In all, we find that the performance of the algae and both roboflagellate configurations are comparable in absolute terms, as measured in terms of body lengths per stroke cycle. This agreement is surprising as we did not precisely match the dimensions of our robots to that of the algal cell, and unlike the algal flagella the robot ‘flagella’ were not capable of active bending [9]—being comprised only of rigid tubing and a plastic hinge.

## 4. Conclusion and future work

Microscopic organisms have evolved to harness many different ways of swimming at low-Reynolds number. Despite their size and simplicity, some single-celled algae can swim with different speeds using gaits analogous to animal gaits, that involve robust temporal ordering of four flagella [20]. Here, we created the very first free-swimming roboflagellate model of these microswimmers to understand how motility and gait influences swimming. Dynamically-scaled robots enable scenarios to be tested that may

not be possible in the live organism [55–58]. Physical modelling has previously provided insights into bacterial swimming [59], flagellar bundling [60], elastic tail propulsion [61], and metachronal actuation of in an on-rail robot with rigid appendages [62].

In contrast, our roboflagellate is self-powered and untethered (no external forces or torques) and was able to achieve fully-3D self-propulsion at low-Reynolds number. The robot recapitulated gait-dependent differences in swimming performance that we measured in the microalgae. These results reveal that phase coordination of propulsive appendages has a significant impact on hydrodynamic performance, while the orientation of appendages relative to the swimmer body also changes propulsion speed. In the perpendicular configuration that most closely models the three algal species studied here, the trot gait was consistently faster than either the pronk or gallop gait. We further predict that quadriflagellates with flagella oriented parallel to the cell body (configuration B) should swim more slowly than the three species studied here, for an equivalent gait. Moreover in all cases the displacement achieved by the robot in terms of body lengths per cycle was similar in absolute terms to the algae. Thus our dynamically-scaled robot is a good locomotor model of the biological microswimmer.

Our work raises open eco-evolutionary questions about the origins of the distinct motility patterns in the different quadriflagellate species. Distinct gaits likely reflect a more nuanced relationship between an organism's metabolic requirements and its habitat. Freely-locomoting organisms at all scales, switch dynamically between multiple gaits [5, 63, 64]. While several *Pyramimonas* species exhibit sporadic bursts of rapid activity with extended quiescent phases [49], *Volvoclean* algae including *Carteria* do not show such rest periods [20]. We conjecture that differences in gait confer an evolutionary advantage even at the microscale. Of the three algae studied here, two (*P. tetra-rhynchus*, *C. carteria*) are freshwater species and one is a marine species (*P. parkeae*). *P. tetra-rhynchus* (type species) was originally isolated from a peaty pool and cultured in a biphasic soil medium [46]. *C. crucifera* is also a freshwater species that forms surface associations with leaves and other decaying material. In contrast *P. parkeae* is most abundant in Arctic surface water and in tidal rock pools, where it can access sufficient sunlight for photosynthesis. *P. parkeae* also exhibits a unique diurnal vertical settling behavior [65]. The latter behavior, along with phototaxis, accentuates the requirement for vigorous swimming and hence the fast trot gait. Field data has shown that marine *Pyramimonas* routinely blooms in and around sea ice, where the unique polar environment (extreme fluctuations in temperature, light, salinity etc) is associated with a highly heterogeneous distribution of different *Pyramimonas* species even within the same water column [66]. The habitats of these algae

may therefore be a key evolutionary driver leading to significant diversification of gait, even across species with apparently convergent morphology and size [67, 68]. Further experiments using both lab strains and wild isolates, controlling more precisely for culturing medium, are need to test this hypothesis. Our roboflagellate model can be used to explore mix-mode propulsion strategies and unsteady effects, such as nutrient dispersal.

We highlight two limitations of the current model. The first concerns boundary and finite-size effects, particularly due to fluid-structure interactions between moving appendages and the bounding tank, and between different parts of the robot. The presence of no-slip boundaries will alter the flow fields around a beating appendage, and change propulsion efficiency [69]. The chiral insertion of the robot flagella around the central body likely introduced an additional (unwanted) rotational movement. Second, the current robot relies on a two-link flagellum facilitated by a rigid 3D printed joint which has fewer degrees of freedom than the organisms. The rigid joints have limited ability to resist torsion—which may be gait-dependent. Eukaryotic flagella and cilia can maintain their shape even when subject to significant hydrodynamic forces. They can also deform actively, to optimise propulsive force generation and efficacy [70, 71]. In future work we can resolve these limitations with more realistic roboflagellate designs, in parallel with hydrodynamic simulations and modelling to understand gait optimisation with truly deformable appendages.

In conclusion, we have presented a macroscopic robot capable of self-propulsion at low-Reynolds number, and used this successfully to model aspects of microorganism swimming behavior. This approach has transformative potential for understanding different mechanisms of microscale swimming, e.g. gait selection, coordination and taxis [18]. These insights could have profound implications for how morphological computation may be achieved in aneural or early nervous systems. From a technological perspective, these diverse propulsion strategies can provide unique, innovative solutions to the formidable challenge of navigating viscous fluids.

## Acknowledgments

The authors are grateful for funding from Physics of Living Systems Student Research Network to KD and DIG, NSF-Simons Southeast Center for Mathematics and Biology (National Science Foundation DMS1764406, Simons Foundation SFARI 594594) to KD, the Dunn Family Professorship (DIG), and from the European Research Council (ERC) under the European Union's Horizon 2020 Research and Innovation Programme (Grant Agreement No. 853560 to

KYW). We also acknowledge the 2018 MBL Physiology Course (Woods Hole, MA) during which this project was conceived.

## Data availability statement

All data that support the findings of this study are included within the article (and any supplementary files).

## ORCID iDs

Daniel I Goldman  <https://orcid.org/0000-0002-6954-9857>

Kirsty Y Wan  <https://orcid.org/0000-0002-0291-328X>

## References

- McNeill Alexander R 2003 *Principles of Animal Locomotion* Student edn (Princeton, NJ: Princeton University Press)
- Chong B et al 2018 Coordination of back bending and leg movements for quadrupedal locomotion *Robotics: Science and Systems* vol 20
- Astley H C et al 2020 Surprising simplicities and syntheses in limbless self-propulsion in sand *J. Exp. Biol.* **223** [jeb103564](https://doi.org/10.1098/jeb103564)
- Purcell E M 1977 Life at low Reynolds number *Am. J. Phys.* **45** 3–11
- Stocker R and Seymour J R 2012 Ecology and physics of bacterial chemotaxis in the ocean *Microbiol. Mol. Biol. Rev.* **76** 792–812
- Rüffer U and Nultsch W 1998 Flagellar coordination in *Chlamydomonas* cells held on micropipettes *Cell Motil.* **41** 297–307
- Wan K Y and Goldstein R E 2016 Coordinated beating of algal flagella is mediated by basal coupling *Proc. Natl Acad. Sci.* **113** 2784E–93
- Theers M and Winkler R G 2014 Effects of thermal fluctuations and fluid compressibility on hydrodynamic synchronization of microrotors at finite oscillatory Reynolds number: a multiparticle collision dynamics simulation study *Soft Matter* **10** 5894–904
- Beeby M, Ferreira J L, Tripp P, Albers S-V and Mitchell D R 2020 Propulsive nanomachines: the convergent evolution of archaella, flagella and cilia *FEMS Microbiol. Rev.* **44** 253–304
- Lauga E 2016 Bacterial hydrodynamics *Annu. Rev. Fluid Mech.* **48** 105–30
- Jahn T L and Votta J J 1972 Locomotion of Protozoa *Annu. Rev. Fluid Mech.* **4** 93
- Blake J R and Sleight M A 1974 Mechanics of ciliary locomotion *Biol. Rev.* **49** 85–125
- Becker L E, Koehler S A and Stone H A 2003 On self-propulsion of micro-machines at low Reynolds number: purcell's three-link swimmer *J. Fluid Mech.* **490** 15–35
- Howse J R, Jones R A L, Ryan A J, Gough T, Vafabakhsh R and Golestanian R 2007 Self-motile colloidal particles: from directed propulsion to random walk *Phys. Rev. Lett.* **99** 048102
- Lauga E and Powers T R 2009 The hydrodynamics of swimming microorganisms *Rep. Prog. Phys.* **72** 096601
- Cohen N and Boyle J H 2010 Swimming at low Reynolds number: a beginners guide to undulatory locomotion *Contemp. Phys.* **51** 103–23
- Zhang T and Goldman D I 2014 The effectiveness of resistive force theory in granular locomotion *Phys. Fluids* **26** 101308
- Wan K Y and Jékely G 2021 Origins of eukaryotic excitability *Phil. Trans. R. Soc. B* **376** 20190758
- Collins J J and Stewart I N 1993 Coupled nonlinear oscillators and the symmetries of animal gaits *J. Nonlinear Sci.* **3** 349–92
- Wan K Y 2020 Synchrony and symmetry-breaking in active flagellar coordination *Phil. Trans. R. Soc. B* **375** 20190393
- Guo H, Man Y, Wan K Y and Kanso E 2021 Intracellular coupling modulates biflagellar synchrony *J. R. Soc. Interface* **18** 20200660
- Sym S, Kawachi M and Inouye I 2000 Diversity of swimming behaviour in *Pyramimonas* (*Prasionophyceae*) *Phycological Research* **48** 149–154
- Nozaki H, Misumi O and Kuroiwa T 2003 Phylogeny of the quadriflagellate *Volvocales* (*Chlorophyceae*) based on chloroplast multigene sequences *Mol. Phylogenet. Evol.* **29** 58–66
- Gompper G et al 2020 The 2020 motile active matter roadmap *J. Phys.: Condens. Matter* **32** 193001
- Koehl M A R 2003 Physical modelling in biomechanics *Phil. Trans. R. Soc. B* **358** 1589–96
- Aguilar J et al 2016 A review on locomotion robophysics: the study of movement at the intersection of robotics, soft matter and dynamical systems *Rep. Prog. Phys.* **79** 110001
- Smith B J H and Usherwood J R 2020 Minimalist analogue robot discovers animal-like walking gaits *Bioinspir. Biomim.* **15** 026004
- Aydin Y O, Rieser J M, Hubicki C M, Savoie W and Goldman D I 2019 Physics approaches to natural locomotion: every robot is an experiment *Robotic Systems and Autonomous Platforms Advances in Materials and Manufacturing* (*Woodhead Publishing in Materials*) ed S M Walsh and M S Strano (Swaston, Cambridge: Woodhead Publishing) pp 109–27
- Palagi S et al 2016 Structured light enables biomimetic swimming and versatile locomotion of photoresponsive soft microrobots *Nat. Mater.* **15** 647–53
- Lum G Z, Ye Z, Dong X, Marvi H, Erin O, Hu W and Sitti M 2016 Shape-programmable magnetic soft matter *Proc. Natl Acad. Sci.* **113** 6007E–15
- Gu H et al 2020 Magnetic cilia carpets with programmable metachronal waves *Nat. Commun.* **11** 2637
- Polotzek K and Friedrich B M 2013 A three-sphere swimmer for flagellar synchronization *New J. Phys.* **15** 045005
- Ali N and Golestanian R 2005 Propulsion at low Reynolds number *J. Phys.: Condens. Matter.* **17** 1203S–8
- Huang H-W, Uslu F E, Katsamba P, Lauga E, Sakar M S and Nelson B J 2019 Adaptive locomotion of artificial microswimmers *Sci. Adv.* **5** eaau1532
- Qiu T, Lee T-C, Mark A G, Morozov K I, Münster R, Mierka O, Turek S, Leshansky A M and Fischer P 2014 Swimming by reciprocal motion at low Reynolds number *Nat. Commun.* **5** 5119
- Kim Y W and Netz R R 2006 Pumping fluids with periodically beating grafted elastic filaments *Phys. Rev. Lett.* **4** 158101
- Vogel R and Stark H 2012 Motor-driven bacterial flagella and buckling instabilities *Eur. Phys. J. E* **35** 15
- Elgeti J and Gompper G 2013 Emergence of metachronal waves in cilia arrays *Proc. Natl Acad. Sci.* **110** 4470–5
- Digumarti K M, Conn A T and Rossiter J 2018 EuMoBot: replicating euglenoid movement in a soft robot *J. R. Soc. Interface* **15** 20180301
- Owaki D, Kano T, Nagasawa K, Tero A and Ishiguro A 2013 Simple robot suggests physical interlimb communication is essential for quadruped walking *J. R. Soc. Interface* **10** 20120669
- Tinevez J-Y, Perry N, Schindelin J, Hoopes G M, Reynolds G D, Laplantine E, Bednarek S Y, Shorte S L and Eliceiri K W 2017 TrackMate: an open and extensible platform for single-particle tracking *Methods* **115** 80–90

- [42] Unknown Scanning electron micrograph of cultured phytoplankton for feeding to the krill: *Pyramimonas gelidicola*, used with permission from the Water Department of Agriculture and the environment, Australian Antarctic Division
- [43] Hedrick T L 2008 Software techniques for two- and three-dimensional kinematic measurements of biological and biomimetic systems *Bioinspir. Biomim.* **3** 034001
- [44] Lembi C A 1975 The fine structure of the flagellar apparatus of *Carteria* *J. Phycol.* **11** 1–9
- [45] Moestrup O and Hill D R A 1991 Studies on the genus *Pyramimonas* (*Prasinophyceae*) from Australian and European waters: *P. propuisa* sp. nov. and *P. mitra* sp. nov. *Phycologia* **30** 13
- [46] Belcher J H 1969 Further observations on the type species of *Pyramimonas* (*P. tetraarhynchus* Schmarada) (*Prasinophyceae*): an examination by light microscopy, together with notes on its taxonomy *Bot. J. Linn. Soc.* **62** 241–53
- [47] Pearson B R and Norris R E 1975 Fine structure of cell division in *Pyramimonas parkeae* Norris and Pearson (*Chlorophyta, Prasinophyceae*) *J. Phycol.* **11** 113–24
- [48] Cortese D and Wan K Y 2021 Control of helical navigation by three-dimensional flagellar beating *Phys. Rev. Lett.* **126** 088003
- [49] Wan K Y and Goldstein R E 2018 Time irreversibility and criticality in the motility of a flagellate microorganism *Phys. Rev. Lett.* **121** 058103
- [50] Shapere A and Wilczek F 1989 Geometry of self-propulsion at low Reynolds number *J. Fluid Mech.* **198** 557
- [51] Or Y 2012 Asymmetry and stability of shape kinematics in microswimmers' motion *Phys. Rev. Lett.* **108** 258101
- [52] Hatton R L, Ding Y, Choset H and Goldman D I 2013 Geometric visualization of self-propulsion in a complex medium *Phys. Rev. Lett.* **110** 078101
- [53] Hoops H J 1993 Flagellar, cellular and organismal polarity in *Volvox carteri* *J. Cell Sci.* **104** 105–17
- [54] Spöring I et al 2018 Hook length of the bacterial flagellum is optimized for maximal stability of the flagellar bundle *PLoS Biol.* **16** e2006989
- [55] Batchelor G 1996 *The Life and Legacy of G I Taylor* (Cambridge: Cambridge University Press)
- [56] Croze O and Peaudecerf F 2016 G I Taylor and the physics of swimming *Cavendish Mag.* **15** 4–5
- [57] Arco R M, Vélez-Cordero J R, Lauga E and Zenit R 2014 Viscous pumping inspired by flexible propulsion *Bioinspir. Biomim.* **9** 036007
- [58] Gravish N and Lauder G V 2018 Robotics-inspired biology *J. Exp. Biol.* **221**
- [59] Thawani A and Tirumkudulu M S 2018 Trajectory of a model bacterium *J. Fluid Mech.* **835** 252–70
- [60] Kim M J, Kim M J, Bird J C, Park J, Powers T R and Breuer K S 2004 Particle image velocimetry experiments on a macro-scale model for bacterial flagellar bundling *Exp. Fluid* **37** 782–8
- [61] Yu T S, Lauga E and Hosoi A E 2006 Experimental investigations of elastic tail propulsion at low Reynolds number *Phys. Fluids* **18** 091701
- [62] Hayashi R and Takagi D 2020 Metachronal swimming with rigid Arms near boundaries *Fluids* **5** 24
- [63] Holmes P, Full R J, Koditschek D and Guckenheimer J 2006 The dynamics of legged locomotion: models, analyses, and challenges *SIAM Rev.* **48** 207–304
- [64] Hildebrand M 1989 The quadrupedal gaits of vertebrates *Bioscience* **39** 766–75
- [65] Griffin N J G and Aken M E 1993 Rhythmic settling behavior in *Pyramimonas parkeae* (*Prasinophyceae*) *J. Phycol.* **29** 9–15
- [66] Haroardtör S, Lundholm N, Moestrup O and Nielsen T G 2014 Description of *Pyramimonas diskoiicola* sp. nov. and the importance of the flagellate *Pyramimonas* (*Prasinophyceae*) in Greenland sea ice during the winter–spring transition *Polar Biol.* **37** 1479–94
- [67] Leliaert F, Smith D R, Moreau H, Herron M D, Verbruggen H, Delwiche C F and De Clerck O 2012 Phylogeny and molecular evolution of the green algae *Crit. Rev. Plant Sci.* **31** 1–46
- [68] Mcfadden G I, Hill D R A and Wetherbee R 1986 A study of the genus *Pyramimonas* (*Prasinophyceae*) from Southeastern Australia *Nord. J. Bot.* **6** 209–34
- [69] Brennen C and Winet H 1977 Fluid-mechanics of propulsion by cilia and flagella *Annu. Rev. Fluid Mech.* **9** 339–98
- [70] Tam D and Hosoi A E 2011 Optimal feeding and swimming gaits of biflagellated organisms *Proc. Natl Acad. Sci.* **108** 1001–6
- [71] Eloy C and Lauga E 2012 Kinematics of the most efficient cilium *Phys. Rev. Lett.* **109** 038101